Results in Surfaces and Interfaces 6 (2022) 100042

Contents lists available at ScienceDirect

Results in Surfaces and Interfaces

journal homepage: www.elsevier.com/locate/rsurfi

Thermal cyclic resistance and long term inter-diffusion properties of slurry aluminide coatings modified with Si

Alina Agüero [a], María José Landeira Østergård [b], Anette N. Hansson [b], Marcos Gutierrez [a,*]

[a] Instituto Nacional de Técnica Aeroespacial, ES-28850, Torrejón de Ardoz Madrid, Spain
[b] Haldor Topsøe A/S, Haldor Topsoe Allé 1, 2800 Kgs. Lyngby, Denmark

ARTICLE INFO

Keywords:
NiAl
Aluminide coating
Ni-base super alloys
Slurry
Microstructure
Interdiffusion
Cyclic oxidation
Si effect

ABSTRACT

High temperature oxidation resistant aluminide coatings fail due to their inability to maintain a protective scale. The corresponding mechanism of protection is based on of forming a thin Al_2O_3 layer, which depends on the availability of Al at the interface with the intermetallic coating. However, the Al content in the coating's surface decreases with time at high temperatures due to interdiffusion with the substrate and/or frequent regeneration of the protective Al_2O_3 scale when it spalls. Si addition is known to enhance the life of Ni aluminide coatings under certain corrosion environments. In an effort to develop a stable, long lasting coating for industrial components exposed to metal dusting, diffusion aluminide coating has been produced by applying Al-Si slurries of various compositions on alloy 601. Aluminide coatings were prepared by applying a water base, Al slurry to which 1, 10 and 20 wt. % of Si were added, followed by a diffusion heat treatment. The microstructures of the coatings were similar, exhibiting an outer layer consisting of an Al-rich β-NiAl matrix, an almost stoichiometric β-NiAl inner layer and an interdiffusion zone between the coating and the alloy. Thermal cyclic tests in air at 1100 °C have demonstrated good adhesion and stability of all coatings. In addition, long term isothermal tests at 850 °C for up to 3 months in air showed high oxidation resistance of the coating but different degree of coating degradation depending on the composition. The coating with the lowest Si addition was the most stable.

1. Introduction

Ni aluminides (Goward and Boone, 1971) are widely used in several industrial sectors, such as for instance gas and aeronautic turbines to prevent high temperature oxidation and hot corrosion (Deevi et al., 1997; Hetmańczyk et al., 2007) as well as chemical and petrochemical plants to prevent metal dusting (Agüero et al., 2011). These coatings are formed by adding Al to the base alloy followed by heat induced interfusion, and as a result, intermetallics of different composition are formed. When exposed to an oxidizing atmosphere at high temperatures, Ni aluminides develop a protective thin alumina scale which is quite resistant to aggressive environments at high temperature. In addition, the coatings must be able to regenerate this scale rapidly if it detaches, and in order to do so, enough Al must be present at the surface for very long durations. Al may be lost due to spallation of the Al rich scale caused by thermal cycles and poor adhesion, and also by further interdiffusion with the substrate (Agüero and Gutiérrez y V. González, 2009). Indeed, one of the major challenges regarding coating stability is the change in composition during service at high temperatures, due to the continuous diffusion of alloying elements from the base metal into the coating and from the coating into the base metal (Galetz et al., 2019; Pillai et al., 2018).

Considerable efforts have been undertaken to improve both the stability of the protective scale and that of the coating regarding degradation by interdiffusion. Adding Si to aluminide coatings is a well-studied example of the existing work undertaken to achieve these goals.

Several authors such as Smialek (1974), Yang et al. (2012), Shirvani et al. (2002) and coworkers found improvements when adding Si to aluminide coatings deposited on superalloys after oxidation in air at 1100 °C. In addition, Si aluminide coatings were more protective that plain aluminide under hot corrosion conditions at 900 °C according to Young and Deadmore (1980). However, some results indicate that different behaviours are obtained with different substrate materials (Agüero et al., 2011).

It has also been found that Si contributes to retard coating substrate interdiffusion as observed by Guzanov et al. (1982) in Mo base alloys, where Si concentrates in the coating-substrate interdiffusion

* Corresponding author.
E-mail addresses: agueroba@inta.es (A. Agüero), mjlo@topsoe.com (M.J. Landeira Østergård), ANNH@topsoe.com (A.N. Hansson), gutierrezdom@inta.es (M. Gutierrez).

https://doi.org/10.1016/j.rsurfi.2022.100042
Received 28 July 2021; Received in revised form 10 January 2022; Accepted 13 January 2022

zone, forming silicides which act as diffusion barriers. A similar effect is observed in Fe aluminide coatings formed on steels, as the Fe_2Al_5 intermetallic layer that forms when hot dipping steels in molten Al, is reduced in thickness when Si is added (Richards et al., 2013). Diffusion is indeed reduced by the presence of Si as suggested by Betford and Boustead (1974) and confirmed by (Wang and Chen, 2006) and Lemmens et al. (2017) and coworkers. Alternative explanations of this behaviour have been proposed by: (a) Nicholls (1964) who stated that Si atoms interact with the crystallographic arrangement of the Fe_2Al_5 phase, (b) Shankar and Apelian (2002) and Zhang et al. (2013) who indicated that Al activity is reduced in the presence of Si, (c) Kurakin (1970) who found the presence of ternary phases acting as diffusion barriers or (d) Springer et al. (2011) and Yin et al. (2013) by a lower energy of activation needed to form the Fe_2Al_5 phase. For instance Yin and collaborators found that the activation energy decreases as the Si content increases when studying the effect of Si in the formation of intermetallics from solid iron and liquid Al. They also found the higher the Si content, the lower the interdiffusion degree and they propose that the reduction of the activation energy might result from the lattice distortion caused by Si atom penetrating into the Fe_2Al_5 phase.

Aluminide diffusion coatings have been very widely used and exhibit important industrial advantages. For instance, they do not exhibit adhesion issues and are produced by several rather low cost application processes which may include heat treatments after application. The main aluminide deposition processes are pack cementation (Houngninou et al., 2004), chemical vapour deposition (CVD) (Adamiak et al., 2016) and hot dipping (Wang, 2006). More recently, slurry application has become a very interesting, practical and cost effective alternative, in particular because it does not require containment as the other three technologies, and it can be applied locally as well as in situ in any industrial environment where the part to be coated will be used or is being fabricated (Agüero et al., 2008; Rasmussen et al., 2008). Slurries are suspensions of Al particles in a liquid, to which a binder is also added to produce a cohesive layer once it is cured. Furthermore, additives are also included to achieve ease of application by controlling of the rheology of the slurry. Application can take place by means of a brush or by spraying, and immersion is also possible. For instance, Kochmanska et al. have studied the effect of Si content in aluminide slurry coatings on austenitic creep-resisting cast steel and identified that the phase composition of the coatings, which is Al/Si ratio dependent, can have a significant influence on the resistance against carburization. They also found out, that the thickness of the coatings depended on the production parameters (mainly on time and temperature), that the ratio Al/Si in the slurry (in the applied range) did not have a significant impact on the thickness of the coating and that the content of aluminium and silicon in the slurry affected the phase components formed in the coatings (Kochmanska, 2018). In addition, Montero and coworkers studied the corrosion behavior of Al and Si-Al slurry coatings on CM 247 nickel base superalloy under air and a under a sulphidation atmosphere and found that Si did not improve the protective behavior of the coatings Si (Montero et al., 2013).

The present work covers the optimization of a Cr VI free, water based, Si modified slurry deposited aluminide, applied unto Ni base alloy IN 601, in order to increase its high temperature chemical stability. The main objective of the work presented here was to demonstrate the stability of the coating when applied to a component exposed to very high temperatures and oxidizing conditions during shutdowns of the plant. The ultimate goal of this coating is to provide long lasting protection both under metal dusting conditions during service and under oxidation conditions and very high temperatures during shutdowns for any component, including heat exchangers exposed to these very aggressive environments. Indeed, these coatings have shown excellent behaviour under metal dusting conditions (Agüero et al., 2019) and it are currently being employed in several commercial plants around the world. The high temperature oxidation under cyclic and isothermal conditions was studied at 1100 °C and 850 °C respectively to determine the optimum Si level.

Table 1
IN601 composition (wt. %)

Alloy	Ni	Cr	Fe	Mn	Si	Al	Cu	Ti	C	Y
601	Rest	25	13	0.2	0.5	1.7	0.5	0.3	0.10	–

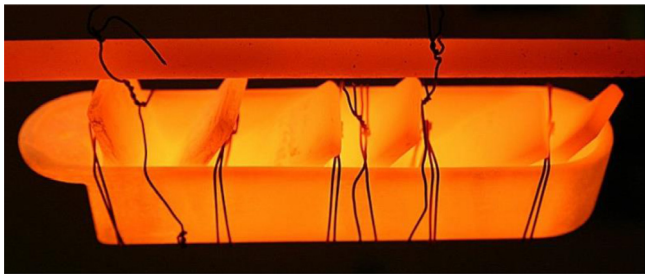

Fig. 1. Images of the cyclic oxidation test rig and the crucible containing specimens during the cooling section of each cycle.

2. Experimental part

2.1. Materials

Sample coupons (20 x 10 x 3 mm) of alloy 601 (UNS N06601) were machined from tubular sections, degreased and blasted with Corundum F46 before testing. The composition of the alloy is shown on Table 1.

Al powder (99.8%; Æ: 4.5 - 5.5 μm) was purchased from Bende-Lutz Werker GmbH, whereas Si powder 99.9% (99.9%; ∅: 1 - 5 μm) was acquired from Alfa Aesar. The ARCAL 10 (Ar 99.999% + 2-5 v. % H_2) gas was obtained from Air Liquid.

2.2. Coating application

The deposition of the Al slurry with a water based, environmentally benign, proprietary binder, was carried out by means of spraying using a Sagola gun followed by drying in air. The wt. % of added Si was calculated relative to the total Al powder present in each slurry composition. After application, the slurry was left to dry under laboratory air at room temperature for 1 h. The dry slurry thickness was approximately 200 μm. The specimens were subjected to a diffusion heat treatment under flowing ARCAL 10 at 700 ° C for 1 h followed by 3 h at 1050 ° C. Slurry undiffused residues were removed by slightly rubbing with a green Scotch-Brite pad.

2.3. Cyclic oxidation testing

This test was carried out at INTA under laboratory air at atmospheric pressure, in a horizontal tubular furnace (PYROX - VG70). During the period in which the test was carried out the humidity in the lab varied within 25%–45%. The samples were placed in crucibles attached to an automatic controlled ceramic arm which took them in and out the furnace in a pre-established cyclic program. Each cycle consisted of a 6 min heating ramp from 50° to 1100 ° C, a 30 min hold at 1100 °C followed by 3 min of forced air-cooling to 50 ° C. Fig. 1 shows the test rig as well as images of the specimens in and out-side the tubular furnace.

The temperature of 1100 °C was selected based on CFD calculations of temperature and flow profiles of the industrial component, which indicate clearly that such high temperatures are expected during plant shutdowns due to back heat from the combustion chamber.

The tests have been conducted under oxidation conditions to simulate the conditions suffered by the industrial component during plant shutdowns.

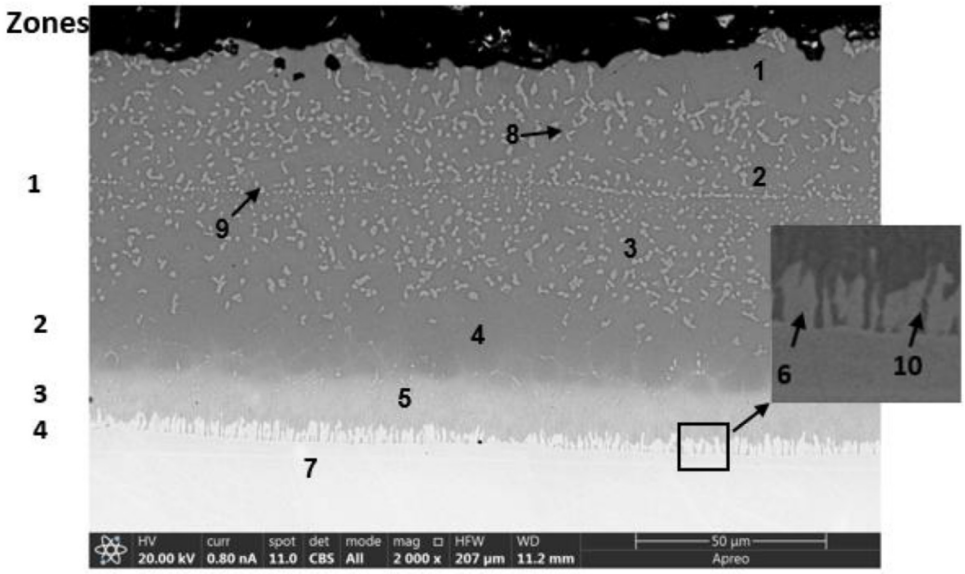

	Al	Si	Cr	Fe	Ni	Ni/Al
Matrix composition (wt. %)						
1	30.5	3.1	7.7	13.5	44.3	1.5
2	31.3	1.6	12.2	11.0	43.8	1.4
3	35.3	0.1	3.7	11.8	48.9	1.4
4	33.7	0.2	6.5	12.5	46.9	1.4
5	17.9	0.4	22.8	10.5	47.7	2.7
6	12.6	0.9	26.9	17.0	45.1	3.6
7	3.2	0.7	24.4	17.0	53.6	16.8
Precipitated phases composition (wt. %)						
8	11.4	11.4	49.2	6.4	21.8	-
9	8.3	12.4	59.3	4.6	14.9	-
10	4.4	0.8	23.3	20.2	50.3	-

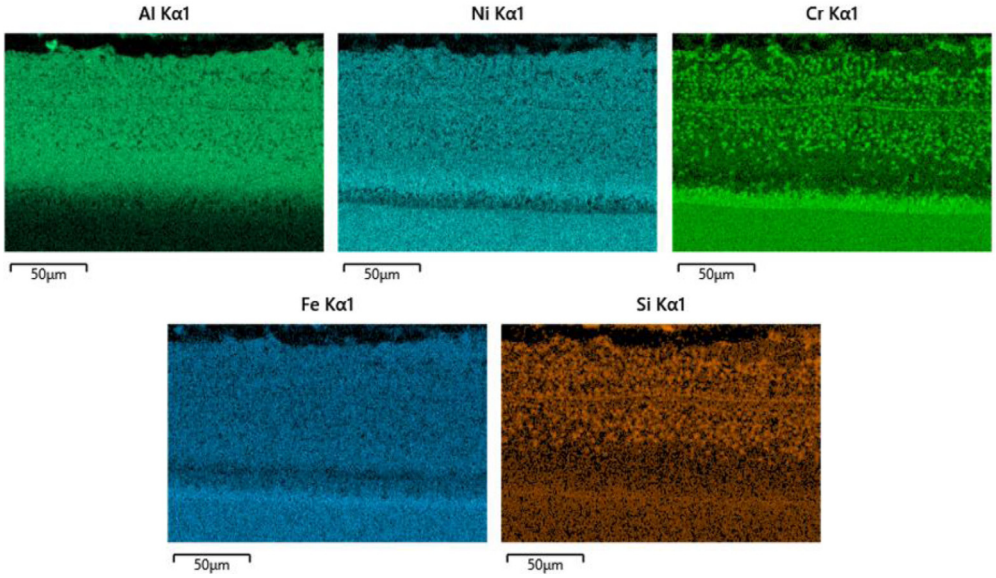

Fig. 2. FESEM image and element mapping of a 1 wt. % Si modified aluminide coating deposited on alloy 601.

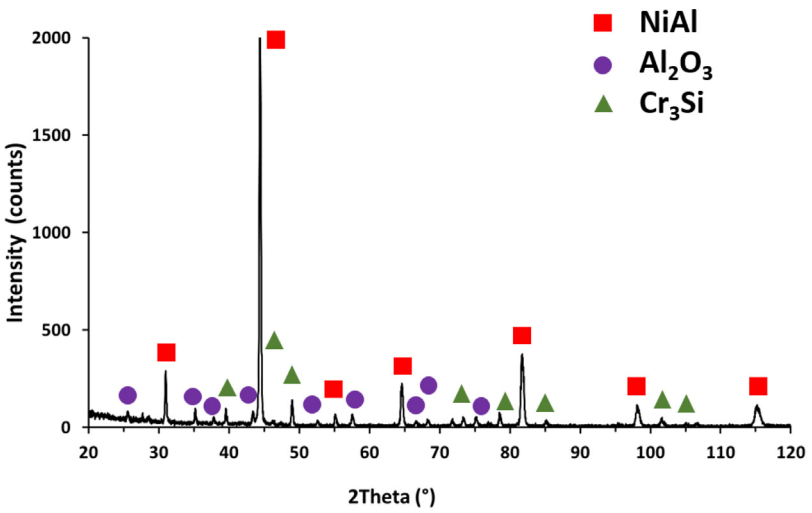

Fig. 3. XRD pattern of the 1 wt. % Si aluminide produced by slurry application on IN 601.

2.4. Isothermal long term aging testing

The isothermal test was carried under laboratory air at atmospheric pressure out at Topsoe on a tubular furnace (Scandia TF 150) at 850 °C for up to 70 days (1680 h). The humidity range is 40%–60%.

This test temperature was chosen to study the stability of the coating composition because 850 °C has been indicated in the literature as the maximum temperature where metal dusting can take place (Grabke, 2003a).

As for thermal cycling, the tests have been conducted under oxidation conditions to simulate the conditions suffered by the industrial component during plant shutdowns.

2.5. Characterization

The coatings were characterized by light microscopy (Leica DV 6) and field emission gun scanning electron microscopy (FESEM) employing a Thermo-Scientific APREO C-LV (ThermoFisher Scientific, Brno, Czech Republic) microscope equipped with an energy-dispersive X ray microanalysis system (EDX) from Aztec Oxford. Cross section observations were obtained by cutting the specimens with a diamond wheel ATM 92002401, mounting them in conductive resin Konductomet (Buehler, Lake Blu, IL, USA) and polishing first with colloidal Si MarterPolish2 (Buehler, Lake Blu, IL, USA) followed by polishing with diamond suspension MetaDi Supreme, Poly, 0.05 μ*m* (Buehler, Lake Blu, IL, USA). The samples were not subjected to etching. Phase composition was examined by X-ray diffraction (XRD) in a Philips X'Pert equipment (Panalytical, Almello, Holland) using the Cu K_ line 0.15418 nm.

The coating thickness was measured in the FESEM employing a 500x magnification and measuring randomly 20 times with an image analyser and then taking the average.

3. Results

3.1. Morphology and microstructure of the as deposited coating

Coatings with 1, 10 and 20 wt. % in Si were prepared by adding Si to the Al slurry (the wt. % was measured relative to the Al powder content). After curing and heat treating the coated specimens for 1 h at 700 °C and 3 h at 1050 °C, the microstructure of the coating with 1 wt. % of added Si consists of four distinct layers as shown in Fig. 2. The thickest, outermost layer (zone 1) appears to be composed of a matrix with a composition matching that of Al rich β-NiAl (Al: 30.5 and Ni: 44.3 in wt. %) in agreement with a very similar coating produced by Rasmussen and collaborators on Inconel 690 also by Al slurry application (without added Si) (Rasmussen et al., 2008). This was confirmed by the corresponding XRD pattern as shown on Fig. 3, which also reveals low intensity peaks attributed to α-Al_2O_3, likely as a result of some degree of oxidation during the coating heat treatment. On this matrix, a second Cr and Si rich phase, constituted by small diameter precipitates can be observed (see the table included in Fig. 2) which tend to appear in grain boundaries. Peaks attributed Cr_3Si are also present in the XRD pattern of this coating and Zang and collaborators observed similar precipitates when they produced an aluminide coating on alloy DZ125 by hot dipping it on an Al–Si (10 wt. %) melt (Zang et al., 2016). Some Si appears also to be dissolved within the matrix (3.1 wt. % near the surface) decreasing in concentration as a function of depth and Cr is also present in the matrix (7.7 wt. %). The next layer (zone 2) has a more homogeneous morphology and a composition gradient with decreasing Al content and as zone 1, exhibits medium size grains. Under zone 2, a significantly larger grain, lighter coloured region, without precipitated phases could be observed (zone 3). Its composition matches Ni rich β-NiAl (Al: 17.9 and Ni: 47.7 in wt. %) with a significant content of dissolved Cr (22.8 wt. %). Large, elongated Cr rich precipitates perpendicular to the surface constitute the innermost zone (4) and were also identified as α-Cr by means of electron diffraction by Rasmussen and collaborators (Rasmussen et al., 2008). This zone is also slightly enriched in Si. The γ'-Ni_3Al phase may be present in the matrix surrounding the Cr rich precipitates as it also contains Al in sufficient amounts. Finally, the substrate placed right under this interdiffusion zone is Ni-depleted due to outwards diffusion of Ni as shown in the corresponding element mapping depicted on Fig. 2.

The morphologies of the other coatings with different Si content are similar but with rougher and more irregular surfaces than the 1 wt. % Si coating.

The coating with 10 wt. % of added Si exhibits the same 4 zones microstructure but with higher Si content at the surface (4.2 wt. %) which also decreases as a function of depth.

Fig. 4 shows the coating with 20 wt. % of added Si. In this case there are differences with the 1 wt. % Si coating, as for instance, the already mentioned very rough and irregular coating surface and the presence of more and apparently smaller Cr and Si rich precipitates within the coating. In addition, the content of Si dissolved in the matrix is significantly higher at the surface (7.9 wt. %) as expected, and also decreases as a function of depth. Moreover, some dark precipitates, very rich in Cr (73.6 wt. %) were observed in zone 3 (β-NiAl). Rasmussen and collaborators identified this phase by electron diffraction in a similar coating deposited on Inconel 690[27]. These precipitates were not observed in the 1 wt. % Si coating. Finally, in zone 4 (interdiffusion

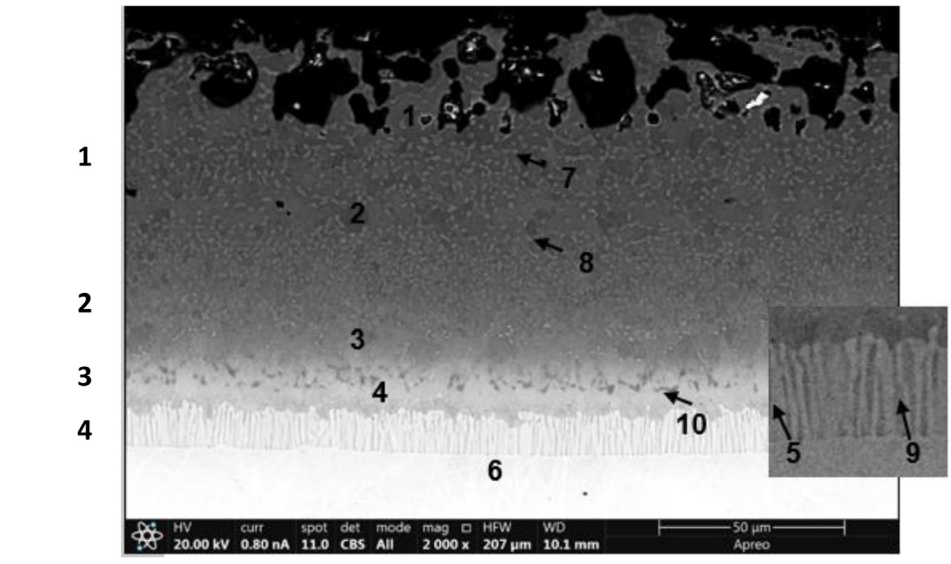

	Al	Si	Cr	Fe	Ni	Ni/Al
Matrix composition (wt. %)						
1	26.7	7.9	1.6	12.3	51.5	1.9
2	27.4	6.7	1.7	14.2	49.8	1.8
3	25.7	3.0	5.0	4.0	60.9	2.4
4	19.1	2.1	4.5	9.9	65.6	3.4
5	11.7	3.2	22.8	14.5	47.0	4.0
6	3.5	2.7	22.0	19.3	51.7	14.8
Precipitated phases composition (wt. %)						
7	10.6	19.6	29.7	11.3	28.3	
8	6.7	20.9	45.5	11.6	15.0	
9	0.9	5.6	48.5	23.3	20.7	-
10	1.9	12.9	73.6	5.6	5.8	

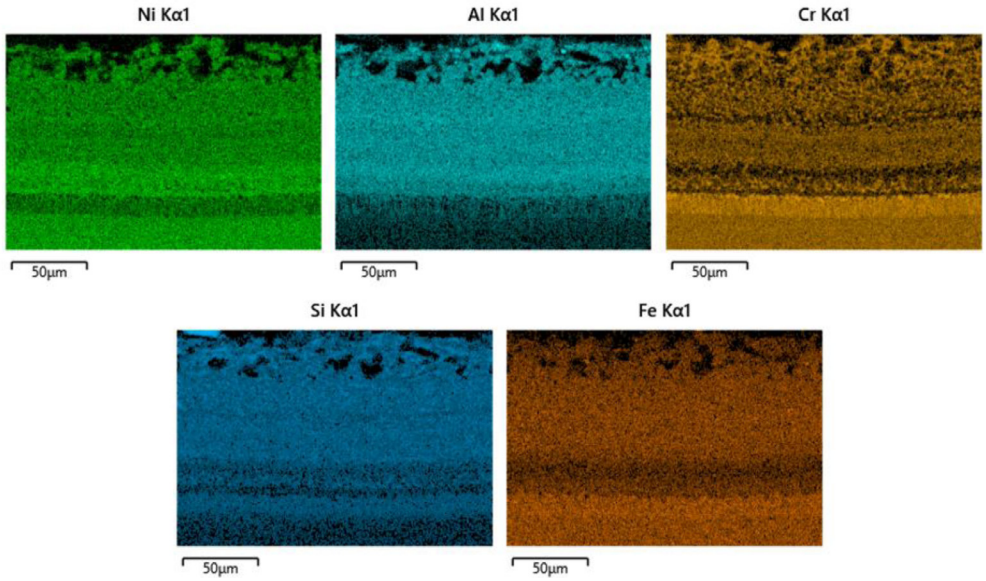

Fig. 4. FESEM image and element mapping of a 20 wt. % Si modified aluminide coating deposited on alloy 601.

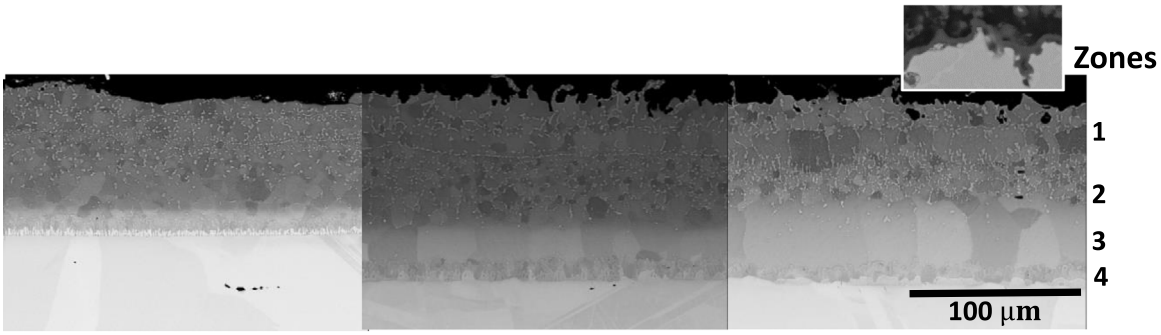

Composition of the aluminide coating near the surface

	Al	Si	Cr	Fe	Ni	Ni/Al
Zone 1 (Matrix)						
to	30.5	3.1	7.7	13.5	44.3	1.5
10 cycles	29.8	0.2	5.3	13.9	50.7	1.7
20 cycles	25.2	0.3	5.7	15.2	53.6	2.1

Fig. 5. FESEM images of the 1 wt. % Si modified aluminide coating deposited on alloy 601 as a function of thermal cycles at 1100 °C.

zone), the elongated features present in the 1 wt. % Si coating appear more defined and longer. The global Si and Cr in this zone is higher than in the 1 wt. % Si. The overall Ni/Al wt. % ratio appears higher in this coating, and the corresponding intermetallic phase also matches β-NiAl, as that observed in the 1 wt. % Si coating.

3.2. Cyclic oxidation

All coatings were subjected to cyclic oxidation testing from 50 to 1100 °C for a total of 20, 0.5 h cycles, for an approximate total duration of 10 h. This very high temperature was chosen in order to accelerate the diffusion process despite being too high for IN 601.

Fig. 5 illustrates the morphology evolution for the coating with 1 wt. % Si after 10 and 20 cycles (~ 5 and 10 h respectively). The coating thickness increased from ~ 88 μm before testing to ~ 130 μm after 10 h at 1100 °C due to Al inwards as well as Ni outwards diffusion. Furthermore, the Al content at the coating's surface decreased from 30.5 to 25.2 (wt. %) with a corresponding increase in the Ni/Al ratio, which went from 1.5 to 2.1 after 10 h (see Fig. 5). As mentioned, this behaviour is typical of Ni aluminide coatings when operating at high temperature. In addition to interdiffusion with the substrate, it could also result from Al loss due to spallation and regeneration of the protective alumina outer scale that these coatings form, which is more pronounced under cyclic conditions due to thermal stresses between the ceramic scale and the metallic coating. It was also observed that the Si content at the surface was significantly reduced as measured in the coating matrix zone. In addition, the morphology has changed in that the thickness of zone 2 (with an Al concentration gradient) decreased, whereas those of zones 1 and 3 (Al and Ni rich β-NiAl respectively) have significantly increased. In addition, the elongated Cr rich precipitates present in zone 4 of the original coating appear to be dissolving in the coating matrix and a new type of coarse large, dark precipitates appear. These are rich in Cr (without Si) and can be identified as α-Cr by analogy to those observed and analysed by Rasmussen and coworkers (Rasmussen et al., 2008) in a similar coating. Cr is known to segregate to grain boundaries and also within Ni–Al phases. A recent phase equilibria study by Nakajima and coworkers (Kitajima et al., 2006) stated that Cr segregates more in the γ'-Ni_3Al phase than in the β-NiAl phase. After cyclic oxidation, the coating surface became quite rumpled and a relatively thin oxide scale developed on top. Rumpling usually appears under thermal cyclic conditions and although the causes are not fully understood, some authors attribute it to local volume changes that take place due to phase transformations as a result of Al content reduction at the surface (Tolpygo and Clarke, 2000). Another proposed rumpling mechanism is based on a combination of lateral growth of the Al rich protective oxide and coating/substrate thermal coefficient mismatch (Chen et al., 2017). Water vapour also can result in creating a rougher surface as proposed by Luo and collaborators who found out by in situ atomic-scale environmental transmission electron microscopy, that in the presence of water vapour, initially surface oxide islands form, which result in localized inward oxide growth into the alloy substrate (Luo et al., 2020).

As shown on Fig. 6, the XRD pattern of the sample exposed to 20 cycles exhibits essentially the same peaks observed in the sample prior to exposure, but the peaks corresponding to α-Al_2O_3 have grown significantly in intensity. This is confirmed by FESEM as shown on Fig. 7, where a thin layer (~1–2 μm) rich in Al and oxygen can be observed on the coating's surface. A high density of Cr and Si rich precipitates is also observed under the protective scale within the coating's β-NiAl matrix.

The evolution of the coating with 10 wt. % Si coating is shown on Fig. 8 and follows a similar behaviour than the 1 wt. % Si coating. In this case the thickness increases from ~ 70 to 105 μm whereas the initial surface Al content is slightly lower than that of the 1% Si sample (26.1 wt. %) and is also reduced (18.5 wt. %) after 20 cycles at 1100° C. Surprisingly and contrary to what was expected, the increment in

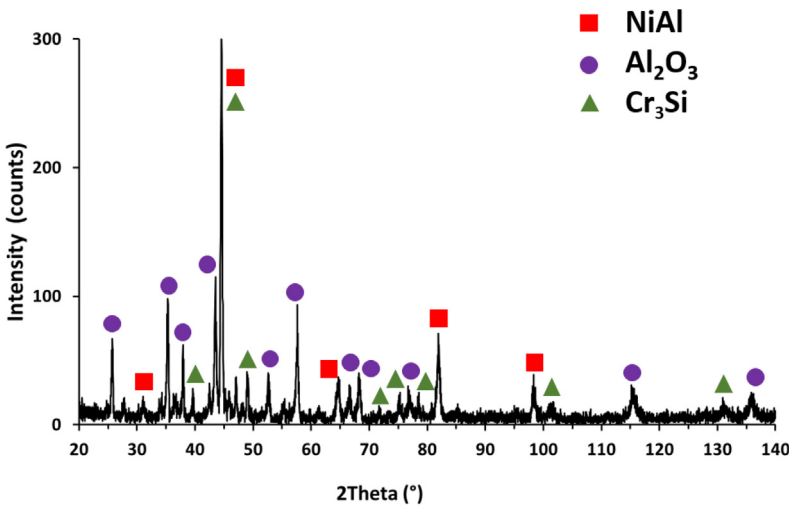

Fig. 6. XRD pattern of the 1 wt. % Si aluminide produced by slurry application on IN 601 after 20 thermal cycles at 1100 ° C.

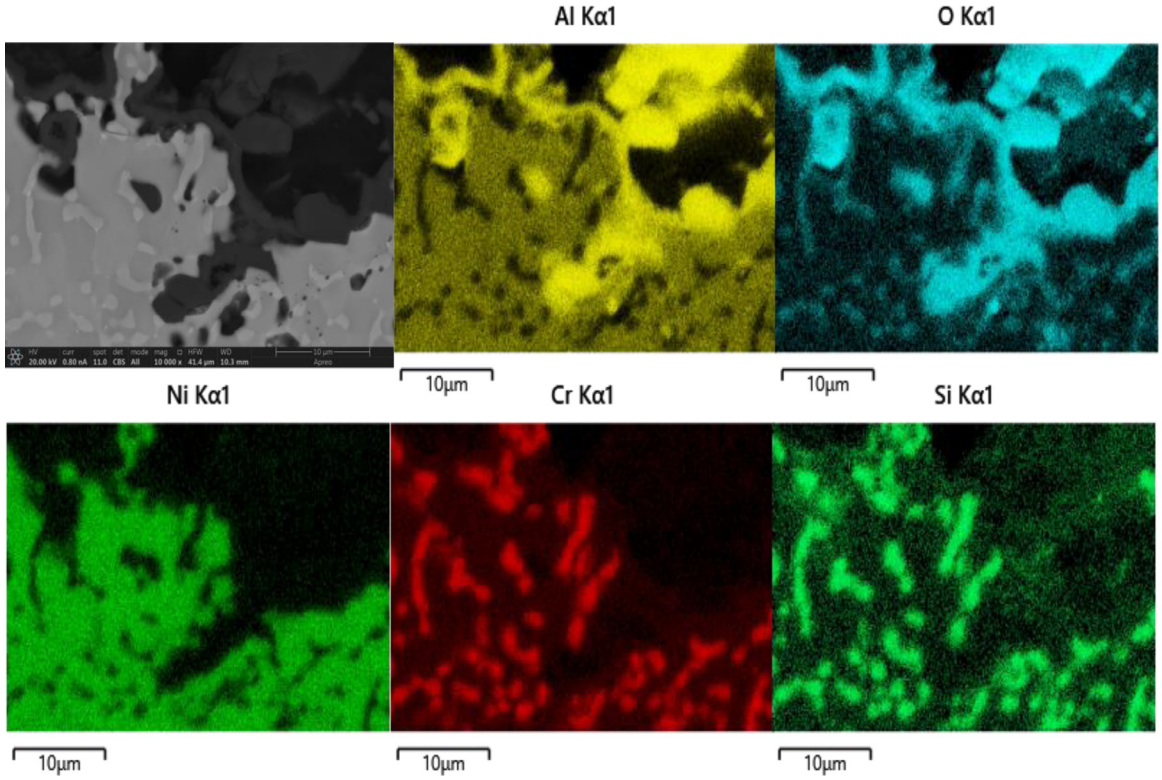

Fig. 7. FESEM image and EDS element mapping of the scale formed on the 1 wt. % Si modified aluminide coating deposited on alloy 601 after 20 thermal cycles at 1100 °C.

the Ni/Al ratio was higher in this case (2.2 to 3.4) indicating a higher reduction of the available Al at the surface. In contrast, in this case the increment in thickness was slightly lower going from ~ 85 μm before testing to ~ 100 μm after 10 h at 1100 °C. As in the previous case, a thin α- Al_2O_3 layer was observed on the coating's surface and there is a detectable increment in the number of Cr rich precipitates that appear at the interdiffusion zone (zone 4).

As shown in Fig. 9, a similar trend was observed in the 20 wt. % Si sample, with an even higher increment in the Ni/Al ratio after 20 cycles (from 1.9 to 4.4) and also a higher increment in thickness (from ~ 95 μm before testing to ~ 150 μm after 20 cycles). However, the Al content at the surface has been reduced after only 10 cycles to ~ 13.5 wt. % and the Si content is approximately twice as high as that in the 10 wt. % Si sample. Moreover, there are notable changes in the microstructure, as for instance, the Al gradient as a function of depth observed in the coatings with lower Si content has disappeared, with the same Al content from the surface and to the interface with zone 4 (~ 13-14 wt. %). In fact the initially present, zones 1 and 2 which exhibited smaller grains have disappeared being replaced by very large grains with low Al content, which are similar to those observed in zone 3 of the original coating microstructure. In addition, the initially present Cr_3Si precipitates seem to have disappeared or perhaps have been transformed into an Al free phase with only 7.0 wt. % in Si and significant amounts of Cr (51.8 wt. %) as well as of Fe (19.4 wt. %) and Ni (20.9 wt. %). This phase is located mainly at grain boundaries

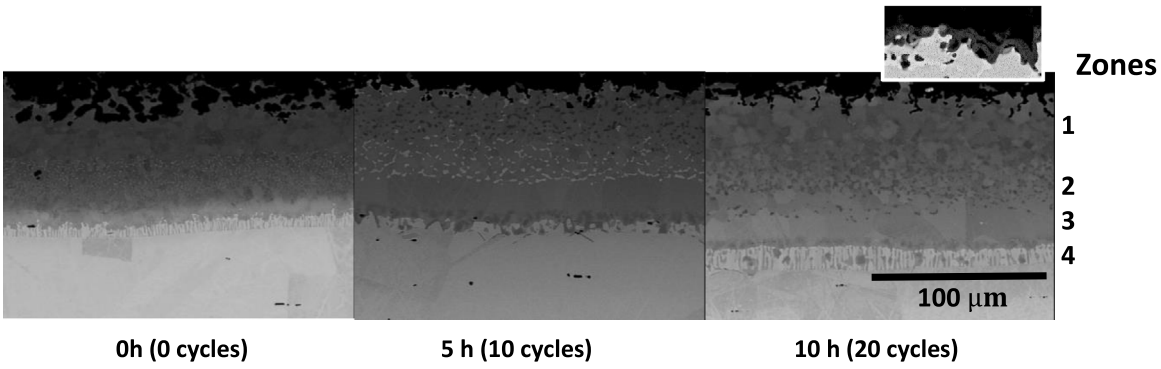

Composition of the aluminide coating near the surface

	Al	Si	Cr	Fe	Ni	Ni/Al
Zone 1 (Matrix)						
to	26.1	4.2	1.8	10.7	57.1	2.2
10 cycles	21.6	2.3	4.9	14.2	56.6	2.6
20 cycles	18.5	1.9	6.7	10.3	63.0	3.4

Fig. 8. FESEM images of the 10 wt. % Si modified aluminide coating deposited on alloy 601 as a function of thermal cycles at 1100 °C.

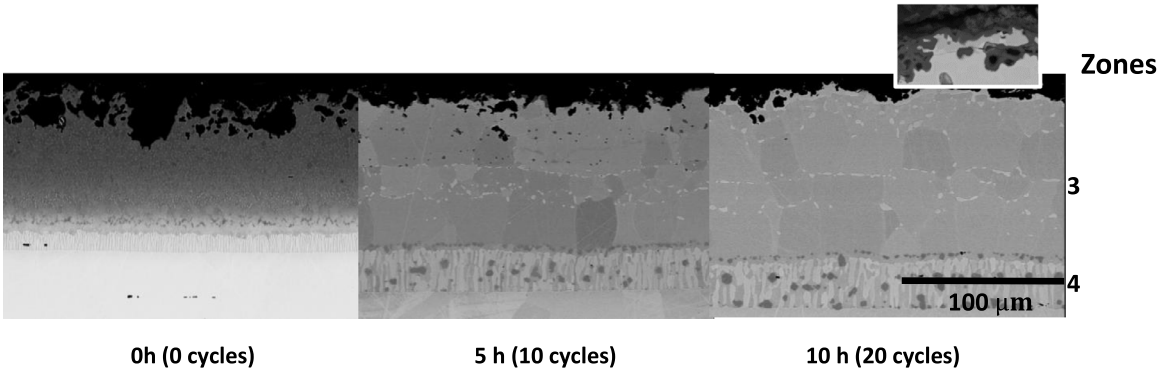

Composition of the aluminide coating near the surface

	Al	Si	Cr	Fe	Ni	Ni/Al
to	26.7	7.9	1.6	12.3	51.1	1.9
10 cycles	13.5	4.1	10.0	11.8	60.5	4.5
20 cycles	13.8	3.8	9.6	11.1	61.2	4.4

Fig. 9. FESEM images of the 20 wt. % Si modified aluminide coating deposited on alloy 601 as a function of thermal cycles at 1100 °C.

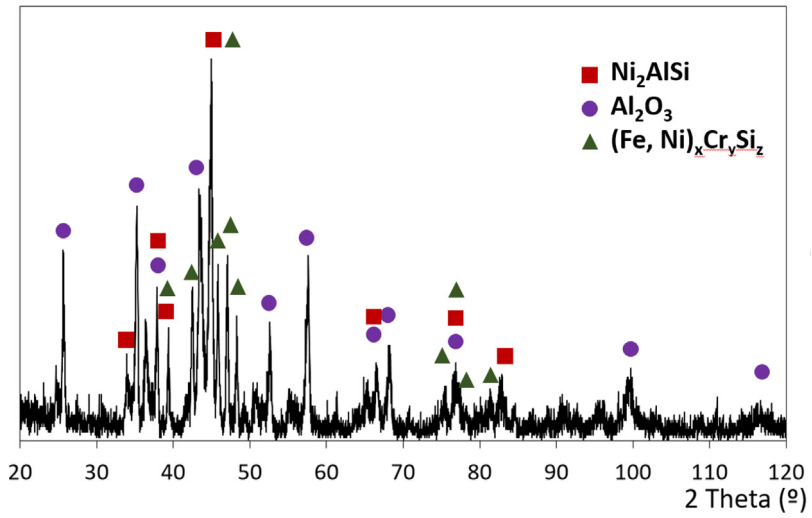

Fig. 10. XRD pattern of the 20 wt. % Si aluminide produced by slurry application on IN 601 after 20 thermal cycles at 1100 ° C.

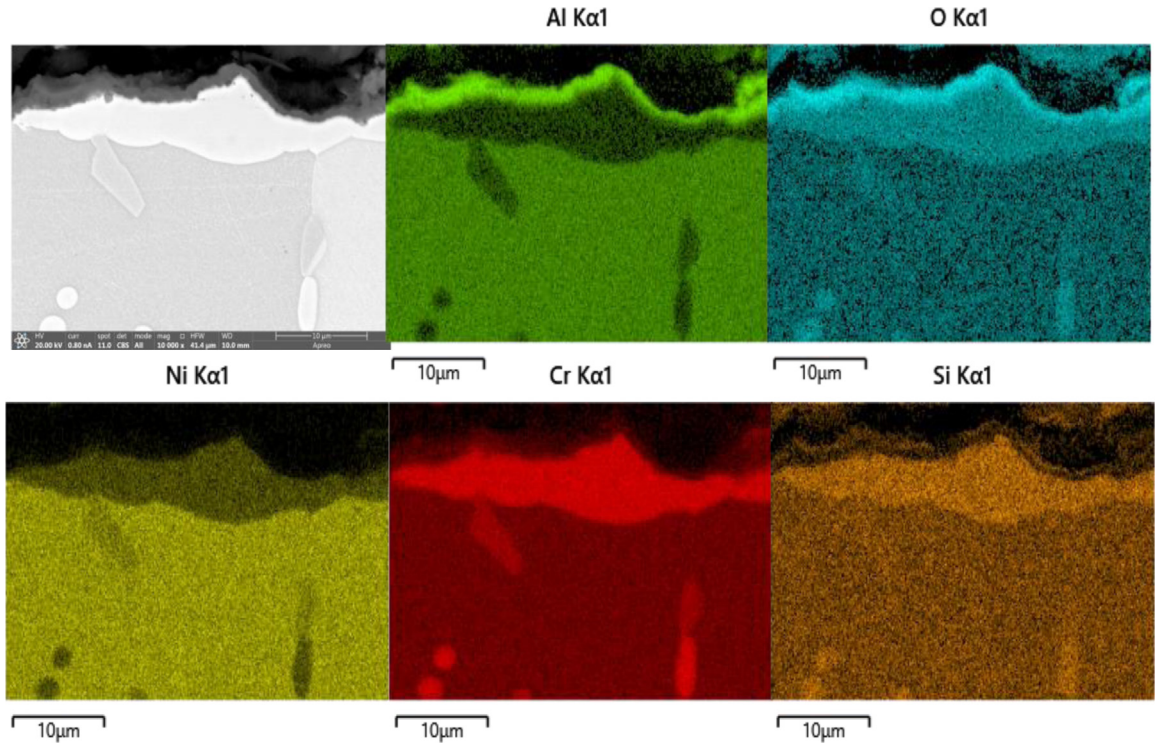

Fig. 11. FESEM image and EDS element mapping of the scale formed on the 20 wt. % Si modified aluminide coating deposited on alloy 601 after 20 thermal cycles at 1100 °C.

within the top half of the coating and in particular, it is also observed under the Al_2O_3 scale after 20 cycles.

The XRD pattern of this sample (Fig. 10) essentially exhibits high intensity peaks corresponding to α-Al_2O_3 (38 wt. % in Al as measured by EDS analysis) with a thickness of ~1-4 μm. Peaks than can be attributed to $AlNi_2Si$ (Ashery and Farag, 2015) were also observed and the EDS analysis also supports the presence of this phase which would likely result from the transformation of the initially present β-NiAl phase due to loss of Al. Several other peaks were present and match the patterns corresponding to $Fe_9Cr_9Si_2$ (Yuan and Wang, 2008), Cr_3Ni_2Si (Buytoz et al., 2013) and/or $Cr_{13}Ni_5Si_2$[37] phases, agreeing with the fact that on most of the coating's surface, the α-Al_2O_3 scale is directly placed on top of the already mentioned Cr, Fe and Ni rich, Al free zone instead of on the Al intermetallic (Fig. 11). In principle, this is not a favourable situation as enough Al must be available right under the protective α-Al_2O_3 scale in order to maintain it, and regenerate it, if it spalls.

In contrast with the other two coatings, on the 20 wt % Si aluminide the α-Al_2O_3 scale and the coating surface seem to have smoothen relative to the initial coating morphology, as seen in Figs. 9 and 11. This is quite unusual as rumpling usually takes place when Ni aluminide coatings are oxidized as mentioned before. Some Si was detected by EDS mapping in the outermost region of the scale indicating that SiO_2 has formed likely by Si diffusion through the remaining α-Al_2O_3 scale perhaps due to lack of sufficient Al on the coating (Fig. 11). Shirvani and coworkers observed also the presence of SiO_2 by XRD on Si enriched aluminide coatings deposited on in 738LC[10]. On the other hand, it is puzzling that hardly any Cr, Ni and Fe were detected within the scale and beyond, so this Al free phase under the scale must be

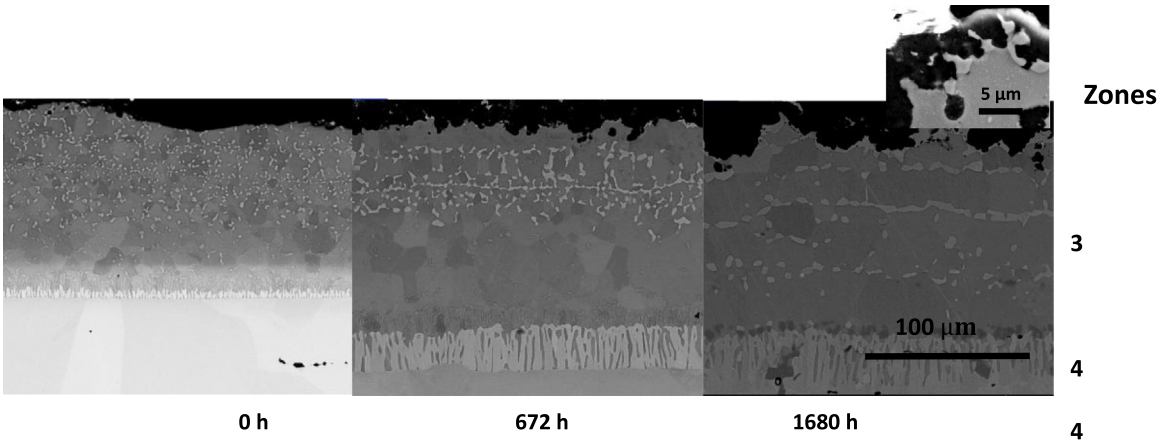

	Al	Si	Cr	Fe	Ni	Ni/Al
to	30.5	3.1	7.7	13.5	44.3	1.5
672 h	27.1	0.4	3.0	6.7	62.9	2.3
1680 h	18.6	0.5	3.7	9.3	67.8	3.6

Fig. 12. FESEM images of the 1 wt. % Si modified aluminide coating deposited on alloy 601 exposed to laboratory air at 850° C as a function of time.

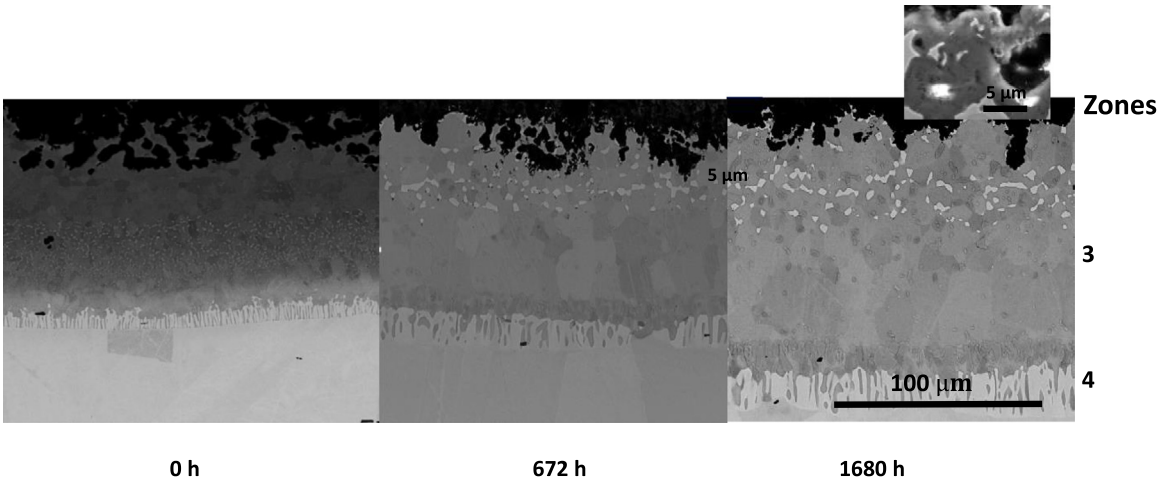

Composition of the aluminide coating near the surface

	Al	Si	Cr	Fe	Ni	Ni/Al
to	26.1	4.2	1.8	10.7	57.1	2.2
672 h	16.9	1.4	3.0	6.7	62.9	3.8
1680 h	16.0	2.3	3.5	9.2	68.4	4.3

Fig. 13. FESEM images of the 10 wt. % Si modified aluminide coating deposited on alloy 601 exposed to laboratory air at 850° C as a function of time.

very stable relative to interdiffusion of these metallic atoms. The large, dark round zones observed in the interdiffusion zones correspond to α-Cr as found in the other coatings after exposure. In this case these particles are significantly more abundant, which may be indicative of an increment of the γ-Ni_3Al phase thickness within the substrate so the lack of sufficient Cr solubility results in precipitation of α-Cr.

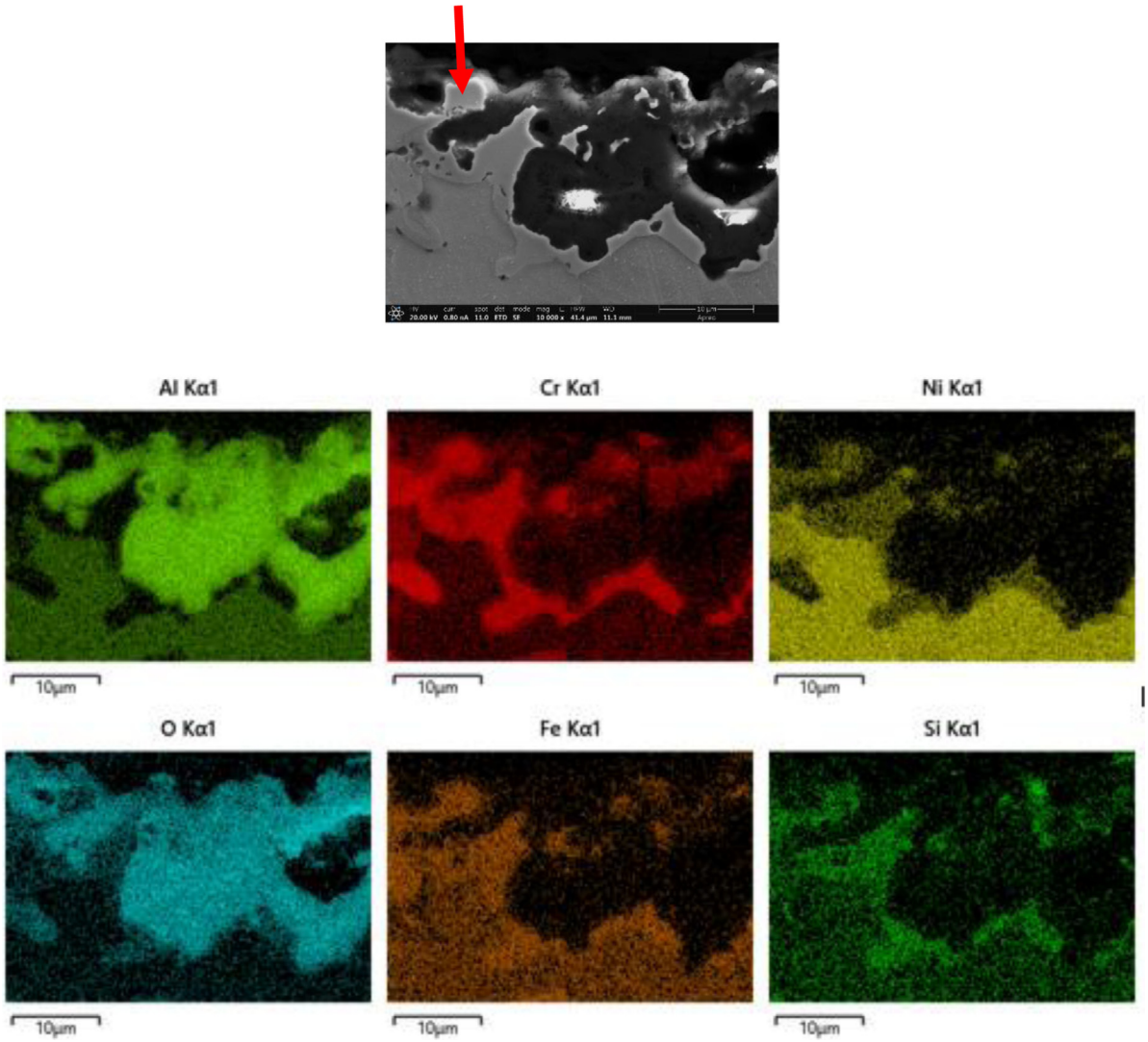

Fig. 14. FESEM image and EDS element mapping of the scale formed on the 10 wt. % Si modified aluminide coating deposited on alloy 601 exposed to laboratory air at 850° C after 1,680 h. The arrow marks a particle almost detached from the intermetallic coating as it is surrounded by oxides.

3.3. Long-term oxidation results

The coatings were also subjected to isothermal, long term exposure under laboratory air for a total of 1,680 h at 850 °C. This temperature was chosen to study the stability of the coating composition because 850 °C has been indicated in literature as the maximum temperature where metal dusting can take place (Grabke, 2003b).

The microstructure evolution of the 1%Si coating at 850° C under air is shown on Fig. 12. The coating thickness apparently increased from 88 to 120 μm after 1,680 h, whereas the Al content at the surface decreased to 18.6 wt. % (from the initial 30.5 wt. %). In analogy with the 20 wt. % Si coating after 20 temperature cycles (only 10 h) at 1100 °C, the Al gradient observed in the original coating disappeared and its content remained constant as a function of depth up to the interdiffusion zone (4). Indeed, the microstructure of these two samples are quite similar, as for the isothermal exposure sample the Cr_3Si precipitates seem also to have disappeared as other light coloured phases appear, now rich in Cr (54,3 wt. %), Fe (25.3 wt. %) and Ni (17.5 wt. %) with only 1.1 wt. % in Si. It can also be observed how the originally small grains at the top, progressively increased resulting in large grains of approximately the same size through the whole thickness of the coating after 1,680 h.

The 10% Si coating exhibited a similar behaviour after 1,680 h of exposure as shown on Fig. 13. For this coating composition, the Al concentration near the surface was reduced from initially 26.1 to 16 wt. % after 1,680 h exposed to air. In this case, the small grain zone fully disappeared faster than in the lower Si coating, as after 672 h all the observed grains were large and of similar size.

In Fig. 14, the element mapping of the coating's outermost surface after 1,680 h, evidences a pure alumina layer which appears to be mostly on top of the Al free phase, rich in Cr (54.9 wt. %), Fe (20.9 wt. %) and Ni (18.9 wt. %) as was also observed in the 20% Si coating exposed to cyclic oxidation (Fig. 9). Some un-oxidized particles from this phase (rich in Si, Fe and Cr) can be observed embedded within the alumina scale, likely resulting from the coating very rough surface as it oxidizes, trapping coating particles. Indeed, on Fig. 14 it can be seen how a particle rich in Cr, Fe and Si is about to be separated from the coating intermetallic phase as it is being surrounded by oxides. As reported by Gleeson, Cheung and Young back in 1993 for high temperature oxidation of Ni–Cr–Al alloys containing Al, Ni and Cr (Gleeson et al., 1993), selective oxidation of Al and the consequent Al depletion under the scale evident from these observations.

Finally, the 20 wt % Si aluminide coating suffered important degradation after 1,680 h as seen on Fig. 15. After 672 h the thickness had increased from initially ~100 to 130 μm and the coating microstructure has substantially changed. From the 4 zones present in the coating prior to exposure only a zone which look similar to zone 3 can be observed. In addition, two very thin, Al poorer phases can be observed

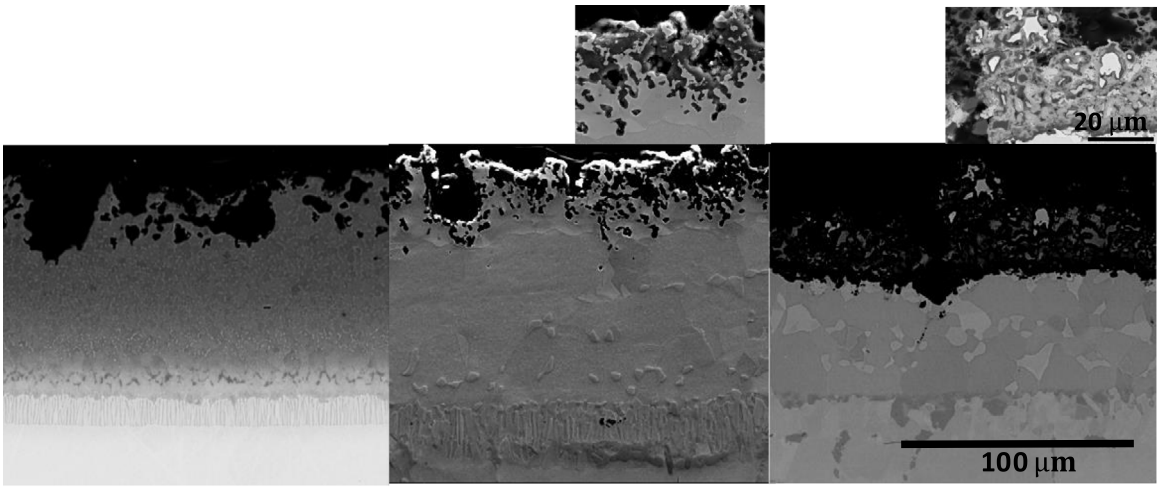

Composition of the aluminide coating near the surface

	Al	Si	Cr	Fe	Ni	Ni/Al
to	26.7	7.9	1.6	12.3	51.5	1.9
672 h	16.5	3.4	4.8	10.2	67.7	4.1
1680 h	15.5	2.1	4.5	7.8	68.7	4.4

Fig. 15. FESEM images of the 20 wt. % Si modified aluminide coating deposited on alloy 601 exposed to laboratory air at 850° C as a function of time.

immediately adjacent to the protective Al_2O_3 scale, as seen on the element mapping shown on Fig. 16a (these are difficult to differentiate in the FESEM image). The phase in direct contact with the protective scale has no Al and is richer in Cr and Si (Cr: 30.5, Si: 10.2, Fe: 17.2 and 41.1 in wt. %) whereas the next one immediately beneath has a very small amount of Al (Al: 2.1, Cr: 19.7, Si: 4.0, Fe: 21.6 and Ni: 52.1 in wt. %). Below these two layers, the measured Al content of the aluminide coating was 15.5 wt. % which is lower than that of the coating's zone 3 prior to exposure (19.1 wt. %) and significantly lower than the original content at the coating's surface (26.7 wt. %).

After 1,680 h the degree of coating degradation is quite high as about half of the coating thickness at 672 h has been lost due to oxidation (Fig. 15). The remaining coating exhibits a constant through-thickness Al concentration profile, all the way to the interdiffusion zone (4) in which the previously existing precipitated phases appear to be dissolving. The Al free phase also found in the other coatings, has grown in volume and now occupies a significant % of the overall intermetallic coating. It appears as it generates within the grain boundaries and then keeps growing as it loses Al due to diffusion. This is also supported by the high content in Cr, as this element tends to accumulate at grain boundaries. Moreover, a thick mixed oxide scale (25-50 μm) with a sponge-like morphology can be observed right above a significantly thinner Al rich scale (Fig. 16b). As in the other coatings, this oxide lays mostly on top of the Al free phase. The thick oxide is rich in Al, Cr, Si as well as Ni, and also contains embedded un-oxidized metallic particles which seem to correspond to the Al free, Cr rich phase and are surrounded by a thin Cr rich oxide. Two different coloured oxide features can be observed: the lighter one is richer in Ni, whereas the darker contains more Si. In fact, given their morphology, the Ni rich oxides seem to result from full oxidation of the metallic particles embedded in the oxide, once the Cr content has been depleted due to the formation of already mentioned Cr rich scale surrounding said particles.

4. Discussion

The results of the oxidation test were totally unexpected as the higher added Si content resulted in a faster degradation of the coatings for the set of compositions prepared in this work within 1 to 20% of added Si.

XRD characterization of the coatings prior to cyclic or isothermal testing has shown the presence of a thin Al_2O_3 layer on the outer surface, see Fig. 3, even though the diffusion heat treatment to form the coating was conducted under reducing conditions in Arcal 10. According to thermodynamics, the oxygen partial pressure needed to form Al_2O_3 at 1050 °C is as low as 10^{-32} atm, and kinetics govern the growth of the oxide layer.

The Al_2O_3 peaks in the XRD spectrum are very small indicating a low thickness of this oxide. This was corroborated by surface SEM/EDS examinations where Al and O were detected, but the layer was too thin to be detected in cross section images. A possible explanation is the fact that the Al slurry is made with a water based binder which after application, was dried in air previous to the heat treatments. It is very likely that some small amounts of water remained within the applied slurry, and that this contributed to the formation of the observed Al_2O_3.

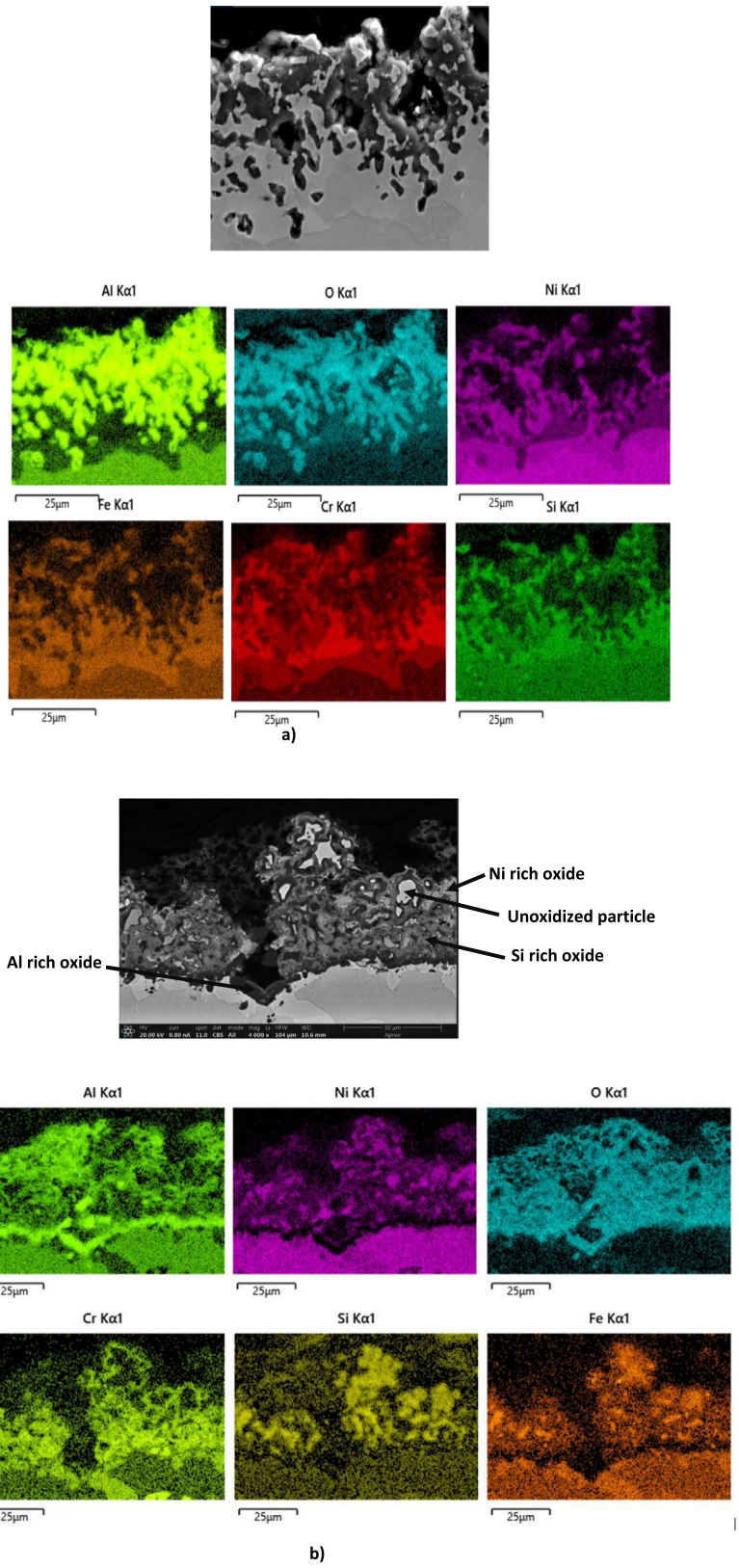

Fig. 16. FESEM images and EDS element mapping of the 20 wt. % Si modified aluminide coatings deposited on alloy 601 exposed to laboratory air at 850 ° C after (a) 672 h and (b) 1680 h.

After coating application and the interdiffusion heat treatment, the coatings with the larger amount of Si show larger roughness compared to the 1% Si sample (compare Figs. 2 and 4). Differences in roughness have been observed by other authors (Galetz et al., 2019) when comparing NiAl with Ge-modified NiAl slurry coatings after heat treatments, roughness being largest for the NiGeAl coating. The authors

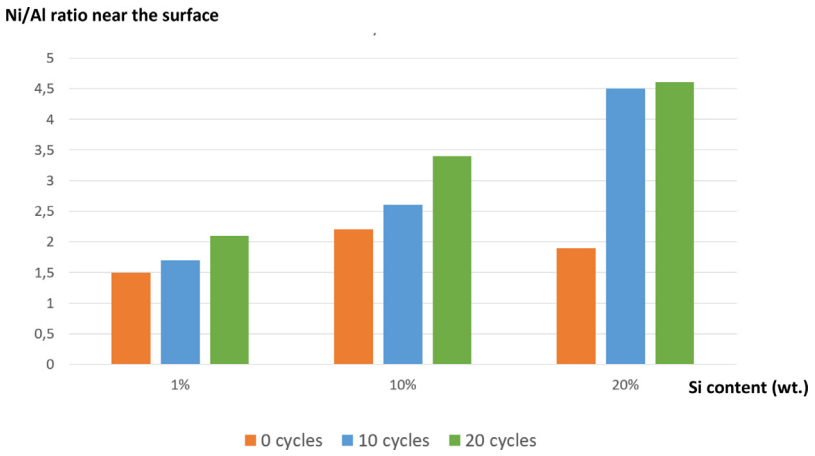

Fig. 17. Surface Ni/Al ratio (in wt. %) of the aluminide coatings with different Si content as a function of thermal cycles at 1100 ° C.

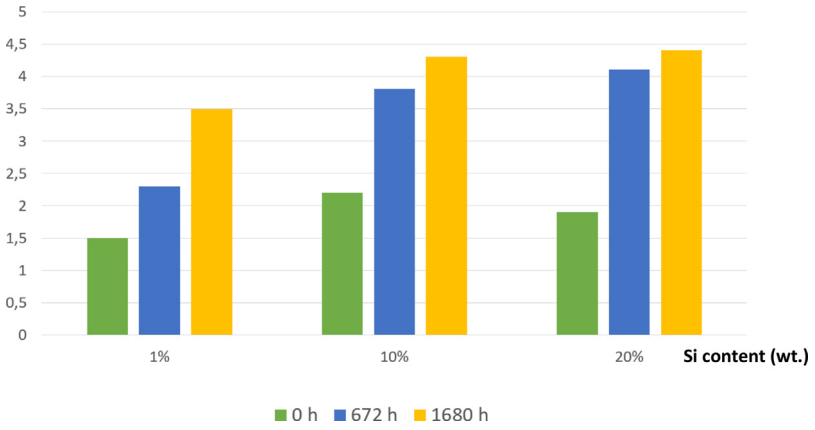

Fig. 18. Surface Ni/Al ratio (in wt. %) of the aluminide coatings with different Si content as a function of time at 850 ° C.

do not discuss nor conclude about the reason for this difference in roughness. The causes for the differences in roughness in the samples with the larger amounts of Si are still under investigation.

Due to coating-substrate interdiffusion and to the development of Al rich protective scales, the initial multi-zone coating microstructure evolves to two zones for the 3 examined Si contents under the two studied oxidation conditions. When comparing the evolution of the Ni/Al ratio as a function of time for each of the studied Si compositions, there is indeed a clear detrimental influence of the Si content as it increases, as shown in Figs. 17 and 18 after thermal cycling and long term isothermal oxidation respectively. A higher Ni/Al ratio implies a lower content of Al available at the coatings' surface and therefore a reduced coating lifetime, since sufficient Al is required to regenerate the protective Al_2O_3 scale when it spalls. Indeed, a higher Ni/Al ratio with time leads to changes in the composition of the Ni-aluminide coating resulting in the transformation of the protective β-NiAl to the non-protective γ'-Ni_3Al.

In Figs. 17 and 18 it can be observed how the Ni/Al ratios increase in the 1 wt. % Si coating under both cyclic and isothermal conditions as a function of time, not reaching a stable value during the tested period. A higher value (3.5) is obtained at the end for the long term isothermal test condition when comparing with the shorter but higher temperature cyclic test during which 2.1 is obtained. In contrast, the 20 wt. % Si aluminide shows a tendency to stabilize reaching a significantly higher ratio (4–4.5) during the two tests, whereas the 10 wt. % coating also shows a tendency to stabilize but at lower rates. These results confirm in the first place, that for the present experiment, the higher the Si content, the higher the Al loss rate, and in the second, that a relatively stable phase composition is reached as a function of time during the tested period for the higher Si coatings.

The increase in thickness experienced by all the tested coatings under both cyclic and isothermal conditions is not too different as a function of composition so higher contents in Si do neither seem to contribute to develop diffusion barriers in this case, nor stabilize the Al rich phases originally present in the coating.

Indeed, interdiffusion alone cannot explain the considerable reduction of the Al content of the coating containing 20 wt. % in Si, so an alternative explanation must be sought. For instance, too much Si might be responsible for a less adhesive Al_2O_3 scale and therefore, regeneration of the spalled scales would cause a faster consumption of Al. In addition the development of Al free, $(Ni, Fe)_xCr_ySi_z$ rich phases located within the coating at grain boundaries and in particular, right below the Al_2O_3 scale is rather puzzling and could have a negative effect in the stability of the scale. On one hand, the lack of Al prevents the scale to regenerate if it spalls, and on the other, these intermetallic phases may be brittle and may lead to easier spallation during thermal cycling. These phases are more abundant in the higher Si content coatings and appear to originate at the β-NiAl grain boundaries, where Cr and Si atoms are known to favourably segregate so that nucleation and growth could take place. Alternatively, these phases could result from Al depletion at the surface of the grains, as diffusion through boundaries is known to be more favourable than through the bulk of the grains.

It was also observed on some of the longer exposed Si richer coatings, the surface tends to smoothen with time, and this may be

explained by the fact that protuberances detach and end up being incorporated in the scale as oxidation surrounds them (see Fig. 14). The particles within the scale may induce faster spallation due to stresses caused by the coefficients of thermal expansion mismatch between the metallic particles and the scale.

In any case, for both cyclic and isothermal exposures increasing the Si content has shown a detrimental effect for the coating stability relative to the 1 Si % containing coating and the main reason for this appears to be a negative effect on the stability of the oxide scale. This is shown in particular, in the 20 wt. % Si sample exposed to 850 °C isothermally for 1680 h where a very thick, Si and Ni rich not very protective scale is developed while the coating is consumed (Fig. 15).

5. Conclusions

The thermal stability of the composition of Si-containing Ni-aluminide coatings formed by slurry application has been studied by thermal cycling and long term oxidation exposures as changes in the composition due to interdiffusion with the substrate at high temperatures will influence the metal dusting resistance of the coating.

The results have shown that increasing the Si content from a 1% wt. Si aluminide coating does not benefit the stability neither when operating at a temperature cycling regime nor under isothermal conditions.

Another interesting finding is the development of Al free, Cr rich Ni, Fe and Si containing phases at the coating's surface on the higher Si content aluminides.

An explanation for this process requires further studies.

On the other hand, the 1 wt. % Si aluminide coating develops a thin protective Al_2O_3 layer and therefore constitutes an excellent candidate for protection of Ni base alloys from metal dusting.

Declaration of competing interest

The authors declare that they have no known competing financial interests or personal relationships that could have appeared to influence the work reported in this paper.

Acknowledgements

AA and MG acknowledge the area of Metallic Materials in INTA for technical support. MJLO & ANNH acknowledge Carsten Rasmussen for assistance with heat treatments.

References

Adamiak, S., Bochnowski, W., Dziedzic, A., Filip, R., Szeregij, E., 2016. Structure and properties of the aluminide coatings on the inconel 625 superalloy. High Temp. Mater. Process. 35, 103–112. http://dx.doi.org/10.1515/htmp-2014-0139.

Agüero, A., Gutiérrez, M., González, V., 2008. Deposition process of steam resistant slurry coatings for new generation high temperature supercritical steam plants. Mater. High Temp. 27, 257–265.

Agüero, A., Gutiérrez, M., Korcakova, L., Nguyen, T.T.M., Hinnemann, B., Saadi, S., 2011. Metal dusting protective coatings. a literature review. Oxid. Met. 76, 23–42. http://dx.doi.org/10.1007/s11085-011-9248-4.

Agüero, A., Gutiérrez, M., Landeira Ostergaard, M.J., Thomsen, S.G., 2019. Burner with a slurry coating with high resistance to metal dusting. ES Patent 1, 2708984A.

Agüero, A., Gutiérrez y V. González, M., 2009. Long term diffusion studies in fe aluminide coatings deposited by slurry application on ferritic steels. Defect Diffus. Forum 289–292, 243–251.

Ashery, A., Farag, A.A.M., 2015. Fabrication, structural and electrical characterization of AlNi2Si based heterojunction grown by LPE. Mater. Sci. Semicond. Process. 35, 66–74. http://dx.doi.org/10.1016/j.mssp.2015.02.052.

Betford, G.M., Boustead, J., 1974. Formation of intermetallic compounds in aluminium-coated steel strip produced by the elphal process. Met. Technol. 1, 233–240. http://dx.doi.org/10.1179/030716974803288167.

Buytoz, S., Ulutan, M., Islak, S., Kurt, B., Nuri Çelik, O., 2013. Microstructural and wear characteristic of high velocity oxygen fuel (HVOF) sprayed nicrbsi-SiC composite coating on SAE 1030 steel. Arab J. Sci. Eng. 38, 1481–1491. http://dx.doi.org/10.1007/s13369-013-0536-y.

Chen, Y., Zhao, X., Bai, M., Yang, L., Li, C., Wang, L., Carr, J.A., Xiao, P., 2017. A mechanistic understanding on rumpling of a NiCoCrAlY bond coat for thermal barrier coating applications. Acta Mater. 128, 31–42. http://dx.doi.org/10.1016/j.actamat.2017.02.003.

Deevi, S.C., Sikka, V.K., Liu, C.T., 1997. Prog. Mater. Sci. 42, 177–192. http://dx.doi.org/10.1016/S0079-6425(97)00014-5.

Galetz, M.C., Oskay, C., Madloch, S., 2019. Microstructural degradation and interdiffusion behavior of NiAl and ge-modified NiAl coatings deposited on alloy 602 CA. Surf. Coat. Technol. 364, 211–217. http://dx.doi.org/10.1016/j.surfcoat.2019.02.048.

Gleeson, B., Cheung, W.H., Young, D.J., 1993. Cyclic oxidation behaviour of two-phase Ni-Cr-Al alloys at 1100 °C. Corros. Sci. 35, 923–929. http://dx.doi.org/10.1016/0010-938X(93)90310-D.

Goward, G.W., Boone, D.H., 1971. Mechanisms of formation of diffusion aluminide coatings on nickel-base superalloys. Oxid. Met. 3, 475–495. http://dx.doi.org/10.1007/BF00604047.

Grabke, H.J., 2003a. Metal dusting. Mater. Corros. 54, 736–746. http://dx.doi.org/10.1002/maco.200303729.

Grabke, H.J., 2003b. Metal dusting. Mater. Corros. 54, 736–746. http://dx.doi.org/10.1002/maco.200303729.

Guzanov, B.N., Kositsyn, S.V., Kuznetsov, V.P., Sorokin, V.G., Orlov, M.R., 1982. Influence of Si on the Protective Properties of Aluminide Coatings, Material Protection of Metals (English Translation of Zashchita Metallov). vol. 18, pp. 114–116, EID: 2-s2.0-0019917397. Part of ISBN: 00331732.

Hetmańczyk, M., Swadźba, L., Mendala, B., 2007. Advanced materials and protective coatings in aero-engines application. J. Achiev. Mater. Manuf. Eng. 24, 372–381.

Houngninou, S., Chevalier, S., Larpin, J.P., 2004. Synthesis and characterisation of pack cemented aluminide coatings on metals. Appl. Surf. Sci. 236, 256–269. http://dx.doi.org/10.1016/j.apsusc.2004.04.026.

Kitajima, Y., Hayashi, S., Narita, T., 2006. Phase equilibria of the nickel-aluminum-chromium system at 1150 °C. Mater. Sci. Forum 522–523, 103–110. http://dx.doi.org/10.4028/www.scientific.net/MSF.522-523.103.

Kochmanska, A.E., 2018. Microstructure of al-si slurry coatings on austenitic high-temperature creep resisting cast steel. Adv. Mater. Sci. Eng. 2018, 5473079. http://dx.doi.org/10.1155/2018/5473079, 12 pages.

Kurakin, A.K., 1970. Mechanism of the influence of si on the processes of the reaction diffusion of iron in aluminium. Phys. Met. Metallogr. 30, 108–114.

Lemmens, B., Springer, H., De Graeve, I., de Strycker, J., Raabe, D., Verbeken, K., 2017. Effect of silicon on the microstructure and growth kinetics of intermetallic phases formed during hot-dip aluminizing of ferritic steel. Surf. Coat. Technol. 319, 104–109. http://dx.doi.org/10.1016/j.surfcoat.2017.03.040.

Luo, L., Li, L., Schreiber, D.K., He, Y., Baer, D.R., Bruemmer, S.M., Wang, C., 2020. Deciphering atomistic mechanisms ofthe gas-solid interfacial reaction during alloy oxidation. Sci. Adv. 6, http://dx.doi.org/10.1126/sciadv.aay8491.

Montero, X., Galetz, M.C., Schütze, M., 2013. Sulphidation behaviour of a Non Harmful Water-Based Al and Al–Si slurry coating on CM247 superalloy. Oxid. Met. 80, 635–649. http://dx.doi.org/10.1007/s11085-013-9412-0.

Nicholls, J.E., 1964. Hot-dipped aluminum coatings. Anti Corros. Methods Mater. 11, 16–21. http://dx.doi.org/10.1108/eb020226.

Pillai, R., Wessel, E., Nowak, W.J., et al., 2018. Predicting effect of base alloy composition on oxidation- and interdiffusion-induced degradation of an MCrAlY Coating. JOM 70, 1520–1526. http://dx.doi.org/10.1007/s11837-018-2950-9.

Rasmussen, A.J., Agüero, A., Gutierrez, M., Landeira Østergård, M.J., 2008. Microstructures of thin and thick slurry aluminide coatings on inconel 690. Surf. Coat. Technol. 202, 1479–1485. http://dx.doi.org/10.1016/j.surfcoat.2007.06.056.

Richards, R.W., Jones, R.D., Clemens, P.D., Clarke, H., 2013. Metallurgy of continuous hot dip aluminizing. Int. Mater. Rev. 39 (5), 191–212. http://dx.doi.org/10.1179/imr.1994.39.5.191.

Shankar, S., Apelian, D., 2002. Die soldering: mechanism of the interface reaction between molten aluminum and tool steel. Metall. Mater. Trans. B 33, 465–476. http://dx.doi.org/10.1007/s11663-002-0057-7.

Shirvani, K., Saremi, M., Nishikata, A., Tsuru, T., 2002. The role of silicon on microstructure and high temperature performance of aluminide coating on superalloy in-738lc. Mater. Trans. 43, 2622–2628.

Smialek, James. L., 1974. Fused silicon-rich coatings for superalloys. In: NASA Technical Memorandum TM X. vol. 3001, https://pdfs.semanticscholar.org/6c28/0df297736e44bc3c2d8858aa2a14a09b5727.pdf_ga2.68334808.855145287.1597838090-739647061.1597838090.

Springer, H., Kostka, A., Payton, E.J., Raabe, D., Kaysser-Pyzalla, A., Eggeter, G., 2011. On the formation and growth of intermetallic phases during interdiffusion between low carbon steel and aluminium alloys. Acta Mater. 59, 1586–1600. http://dx.doi.org/10.1016/j.actamat.2010.11.023.

Tolpygo, V.K., Clarke, D.R., 2000. Surface rumpling of a (Ni, Pt)Al bond coat induced by cyclic oxidation. Acta Mater. 48, 3283–3293. http://dx.doi.org/10.1016/S1359-6454(00)00156-7.

Wang, C.J., 2006. Microstructure and cyclic oxidation behavior of hot dip aluminized coating on Ni-base superalloy inconel 718. Surf. Coat. Technol. 201, 3862–3866. http://dx.doi.org/10.1016/j.surfcoat.2006.07.242.

Wang, C.J., Chen, S.M., 2006. The high temperature behaviour of hot-dipping Al-Si coating on low carbo steel. Surf. Coat. Technol. 200, 6601–6605. http://dx.doi.org/10.1016/j.surfcoat.2005.11.031.

Yang, R., Yuxiao, Y., Li, S., Ma, Y., Gong, S., 2012. Microstructure of modified aluminide coating on ni3al-based single crystal superalloy. Chin. J. Aeronaut. 25, 825–830. http://dx.doi.org/10.1016/S1000-9361(11)60451-2.

Yin, F.C., Zhao, M.X., Liu, Y.X., Han, W., Li, Z., 2013. Effect of si on growth kinetics of intermetallic compounds during reaction between solid iron and molten aluminium. rans. Nonferr. Met. Soc. China 23, 556–561. http://dx.doi.org/10.1016/S1003-6326(13)62499-1.

Young, S.G., Deadmore, D., 1980. An experimental low cost silicon/aluminide high temperature coating for superalloys. Thin Solid Films 73, 373–378. http://dx.doi.org/10.1016/0040-6090(80)90502-7.

Yuan, Y., Wang, H.M., 2008. A wear and corrosion resistant α-ferrite toughened Fe9Cr9Si2 ternary intermetallic alloy. J. Alloys Compd. 459, 148–154. http://dx.doi.org/10.1016/j.jallcom.2007.04.243.

Zang, J., Song, P., Feng, J., Xiong, X., Chen, R., Liu, G., Lu, J., 2016. Oxidation behaviour of the nickel-based superalloy DZ 125 hot-dipped with Al coatings doped by Si. Corros. Sci. 112, 170–179. http://dx.doi.org/10.1016/j.corsci.2016.07.020.

Zhang, X.B.K., Li, Y., Liu, Y., Yang, C., 2013. New evidence for the formation and growth mechanism of the intermetallic phase formed at the Fe/Al interface. J. Mater. Res. 28, 3279–3287. http://dx.doi.org/10.1557/jmr.2013.345.